Density functional theory study of some structural and energetic properties of small lithium clusters

Georges Gardet, François Rogemond, and Henry Chermette

Citation: J. Chem. Phys. **105**, 9933 (1996); doi: 10.1063/1.472826
View online: http://dx.doi.org/10.1063/1.472826
View Table of Contents: http://jcp.aip.org/resource/1/JCPSA6/v105/i22
Published by the American Institute of Physics.

Density functional theory study of some structural and energetic properties of small lithium clusters

Georges Gardet,[a] François Rogemond, and Henry Chermette
Laboratoire de Chimie-Physique théorique, Université Claude Bernard Lyon 1, 43, Bd du 11 Novembre 1918, F-69622 Villeurbanne Cedex, France and Institut de Recherches sur la Catalyse, CNRS UPR 5401, 2 avenue Einstein, F-69626 Villeurbanne Cedex, France

(Received 2 August 1995; accepted 9 September 1996)

Some properties of small Li_n clusters (n up to 20) are theoretically investigated, within the density functional theory formalism. The structural properties are examined at the so-called local level of approximation. For very small clusters ($n \leqslant 8$), the Li_n conformations which are well known from *ab initio* calculations are found at very low computational cost. For $n > 8$, optimal starting geometries are generated from two growth patterns, based on the increase of the number of pentagonal subunits in the clusters by adsorption of one or two Li atoms. Several new stable structures are proposed, for which the corresponding vibrational analysis is performed for n up to 18. The study of energetic properties and stability requires the use of gradient-approximated functionals. Such functionals are used for the determination of the relative stability of these clusters. For example, we show that the icosahedral structure is the most favorable geometry for Li_{13}, whereas this is not the case for Na_{13}. Ionization potentials and binding energies are also investigated in regard to the size and the geometry of the clusters. Comparison with experimental results and other theoretical approaches (such as nonspherical jellium model) suggests that some combinations of gradient-corrected functionals are more adapted than others to describe Li_n energetic and structural properties. © *1996 American Institute of Physics.* [S0021-9606(96)02746-8]

I. INTRODUCTION

Alkali-metal clusters have become a subject of great interest in condensed matter physics. Many interesting phenomena have been observed during the past decade by experimental groups.[1–9] For example, several experimental data are available for Li clusters,[3,7–9] which provided not only energetic properties but also oscillator strengths and ionization potentials (IP) for Li_3–Li_{10} clusters.

It is interesting to notice that sodium and lithium clusters consisting in the same number of atoms may exhibit very different electronic properties.[3] Whereas the jellium model has been used with success for the understanding of the structures and properties of sodium clusters,[4,10,11] it does not work so well for the corresponding lithium clusters.[7,8] Such behavior prevents any use of too large approximations in the quantum model to study these systems, so that theoretical investigations have only recently been performed. Most of them belong to the *ab initio* numerical technique family,[12–14] which has to be understood as Hartree–Fock plus configuration interaction methods.

More approximated methods like a Hückel-type one,[15,16] lead to some relative stabilities of alkali-metal clusters which will be compared to our calculations, besides the results based on the Hartree–Fock (HF) method in its standard formulation,[12] and within a derived formalism like the localized-orbital HF model of Sugino and Kamimura.[17]

However, the computational effort of the *ab initio* methods is considerable and this has limited such studies to clusters with ten atoms or less so far. On the other hand, density functional methods provide an interesting alternative way since, in the Kohn–Sham formulation,[18] the computational effort scales as n^3, where n is the electron number. These methods use one of several approximations for the exchange-correlation energy, the simplest being the local spin density approximation (LSDA).[19] In most cases the LSDA has proven to lead to quite reliable bond lengths, i.e., geometrical structures. Therefore, the first principle molecular dynamics method,[20] which involves the LSDA in its present formulation, may lead to quite reasonable equilibrium geometries and has already been used in some works.[21] Unfortunately, this is too crude an approximation for energetic quantities, and bonding energies for example are typically overestimated by 100%.[22–24] The use of gradient-approximated (also called gradient-corrected) exchange-correlation functionals has recently allowed the obtention of reasonable bond energies, typically of a few percents of the experiment.[22] Some gradient-corrected exchange-correlation functionals have emerged to be more satisfactory than others, but no general consensus has yet been reached in order to tell which is the best combination of exchange and correlation gradient-corrected functionals.[25] In this work, we use some combinations of the most popular, namely Perdew and Wang (1986) (PW86),[26] Becke (1988) (B88),[27] or Perdew and Wang (1991) (PW91)[28] functions for exchange, and Perdew (1986) (P86),[29] Lee, Yang, and Parr (1988) (LYP),[30] or Perdew and Wang (1991) (PW91)[28] functions for correlation. They are local functionals of both the density and its gradient. For this reason, they are often called gradient-corrected functionals in the literature, and throughout this paper; this does not mean

[a]Present address: Institut de Physique et de Technologies du Vide IUT de Saint-Etienne, 28 Av Léon-Jouhaux F-42023 Saint-Etienne Cedex 2, France.

they are perfectly correct because of the use of density gradients in their formulation. Following Perdew, some authors prefer to call them generalized gradient approximation (GGA), whereas others called them ''nonlocal spin density functionals'' (NLSD) because a part of the nonlocality is described by the gradient term. This is misleading, although we have also used the acronym NLSD in this paper.

The aim of this study is to examine whether the density functional theory (DFT), within the present state of art of gradient corrected functionals, is able to reproduce (at lower cost) the theoretical data and/or experimental data of small clusters, and allow prediction of properties of bigger clusters. Remember that if experimental data are available for optical spectra, IP, or relative abundance in mass spectra, no experimental data by itself is a signature of the geometrical structure of the most stable isomer. Moreover, the obtention of these clusters from a laser ablation source, which produces relatively hot clusters, does not prevent a possible coexistence of different isomers in the beam. Theoretical relative energies of clusters should bring some understanding in the mechanism of growth of clusters, while theoretical absorption spectra of given structures should help in the assignment of experimental spectra to definite structures.[31–34]

II. STRUCTURAL PROPERTIES

A. Computational details

All calculations are made with deMon[35] and/or ADF codes[36] with both the Dirac–Vosko Wilk Nusair (Dirac–VWN) LSD exchange-correlation functional[37,38] and with some of the most popular gradient-corrected functionals already cited (in the following, a X-Y combination of functionals refers to X for the exchange part and to Y for the correlation part). For all sizes, except 19 and 20, no symmetry constraint was applied during the geometry optimization process. In all cases, we used with deMon the Gaussian orbital basis set named DZP2 (721/1*/1+) proposed by Godbout *et al.*[39] The auxiliary basis set used for fitting the density and the exchange-correlation potential follows the (4,3;4,3) pattern. We have checked, using some small clusters, that these Gaussian basis sets are sufficient for the obtention of geometries and the related properties analyzed here. For ADF, the Slater basis (orbital and auxiliary sets) named V-Li.1s has been used. Since this basis set includes f-type orbitals, it is more extended than the Gaussian (721/1*/1+) one, but the 1s orbital is kept frozen, contrary to the case of the deMon calculations which are all electrons.

B. Very small clusters ($n \leqslant 8$)

The conformations of very small lithium clusters are already known from *ab initio* investigations.[12,32] They are recovered within our DFT calculations, including both the LSD and gradient-corrected levels of approximation. It is worthwhile to note that, in most cases, these geometries are recovered at the LSD level, which is cheaper in computing time. These conformations, which are gathered in Fig. 1(a), have been optimized, in a first step, at the LSD level of approximation (Dirac–VWN) with deMon or ADF codes. Then these structures were self-consistently optimized with the B88LYP and B88P86 gradient-corrected functionals through deMon program. Table I contains the corresponding interatomic distances.

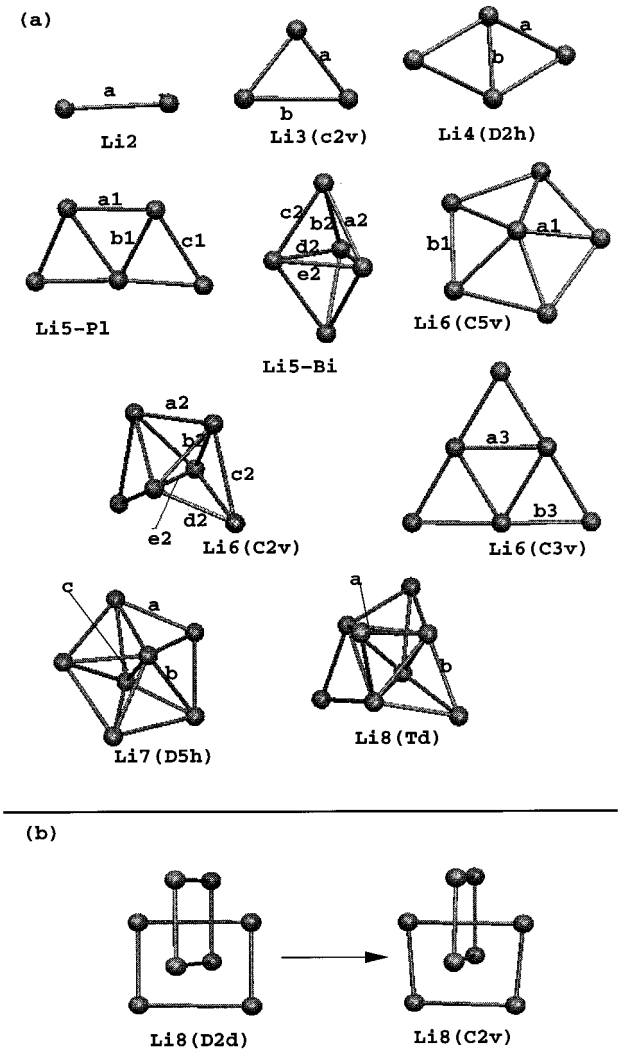

FIG. 1. (a) Geometrical structures of small Li_n clusters ($n \leqslant 8$). The interatomic distances are labelled according to Table I. (b) $Li_8(D_{2d})$ structure proposed by Blanc *et al.* (Ref. 32) optimized at the LSD level and without symmetry constraints relaxes towards $Li_8(C_{2v})$ structure.

Differences between the two DFT codes used for our LSD structures remain small [rms deviation for the interatomic distances of about 2% (Table I)]. They originate mainly in the difference in the basis sets (Gaussian- or Slater-type, respectively) and their spatial expansions, and in the different fits of the electron density.

More important is the comparison with the *ab initio* calculations. Most stable geometries at the local level of approximation are quite similar to those of the very accurate *ab initio* calculations of Ref. 12. Such a good behavior of LDA in geometry optimizations has already been pointed out in earlier works.[40] Here, only two clusters [Li_3 and $Li_6(C_{2v})$] exhibit interatomic distances somewhat different from those given in Ref. 12: one distance is strongly underestimated in

TABLE I. Interatomic distances (in pm) calculated with LSD (Dirac–VWN) and two NLSD (B88-LYP and B88-P86) functionals. The letters $a,b,\ldots,a1,b1,\ldots,a2,b2,\ldots$, correspond to Fig. 1. We have used two DFT codes to optimize geometrical structures: deMon (Ref. 35) and ADF (Ref. 36). CI results are those of Boustani *et al.* (Ref. 12) the values marked with (A) and (B) letters excepted, which correspond to Ref. 49 and Ref. 31, respectively.

pm	CI	Dirac–VWN ADF	Dirac–VWN deMon	B88LYP deMon	B88P86 deMon
Li_2:a	265[(A)]	274	277	274	278
$Li_3(C_{2v})$:a	289	281	285	285	286
b	397	338	350	393	352
$Li_4(D_{2h})$:a	316	306	312	309	318
b	269	263	270	264	269
Li_5-Pl:$a1$	308	307	314	308	314
$b1$	308	288	298	299	301
$c1$	309	299	304	305	306
Li_5-Bi:$a2$	328	310	314	315	314
$b2$	312	298	302	301	302
$c2$	328	310	314	316	314
$d2$	281	271	274	270	277
$e2$	339	311	319	330	318
$Li_6(C_{5v})$:$a1$	294	285	291	287	292
$b1$	333	314	319	323	324
$Li_6(C_{2v})$:$a2$	322[(B)]	354	363	362	318
$b2$	305[(B)]	282	288	288	297
$c2$	366[(B)]	354	361	364	347
$d2$	308[(B)]	282	288	288	298
$e2$	264[(B)]	260	265	260	262
$Li_6(C_{3v})$:$a3$	319	298	308	309	311
$b3$	311	298	303	302	306
$Li_7(D_{5h})$:a	315	304	308	308	310
b	310	294	299	299	301
c	310	280	287	287	290
$Li_8(T_d)$:a	309	290	295	293	297
b	311	297	302	305	306

Li_3, i.e., 350 pm compared to 397 pm in Ref. 12, and the reverse is found in $Li_6(C_{2v})$ (363 and 322 pm, respectively). Whereas LDA geometries are quite satisfactory, the use of gradient-corrected functionals does not yield important deformations (and, of course, to other stable structures). Indeed, the interatomic distances are only slightly modified, except in the critical cases of Li_3 and $Li_6(C_{2v})$ where they are considerably improved, although the improvement depends on the selected NLSD functional (Table I).

C. Small Li_n clusters geometries ($n>8$)

1. Introduction

In some recent works,[16,21] the Born–Oppenheimer energy surface of Na_n clusters have been scanned extensively showing, for each size $6\leqslant n\leqslant 21$, a systematic presence of pentagonal bipyramids (PBP) subunits among the more stable isomers. Moreover, structures containing the greatest number of PBP subunits (''PBP structures'') are stable Li_n clusters too, when $n=9,10,12,14,19,30,40$.[12,17,41,42] Accordingly, such a behavior can be expected for $n=11,13,18,20$. For these sizes, new PBP structures were proposed within two pentagonal growth mechanisms.

2. Pentagonal growth pattern involving the addition of two Li atoms

We examine a growth pattern based upon the addition of a Li_2 dimer to build a new PBP (part B of Fig. 2). This addition is reasonable because of the large abundance of this dimer observed in experimental molecular beams.[8]

The smallest optimal geometry containing one PBP is $Li_7(D_{5h})$. Because of the high symmetry, there is only one possibility to obtain $Li_9[Li_9(C_s)]$ with a second PBP. Then there are seven different paths to build Li_{11}. Two of them have been taken into account in our calculations and the corresponding optimized Li_{11} structures contain 3 PBP ($Li_{11}A$ and $Li_{11}B$). Finally, from $Li_{11}A$ we obtained a Li_{13} structure with four PBP: $Li_{13}(C_s)$ (Fig. 3).

3. Pentagonal growth pattern by addition of a single Li atom

To obtain a pentagon by addition of a single Li atom, the four starting atoms must lie approximately in the same plane, and it is a demanding constraint (part C of Fig. 2). Nevertheless, there exist a smaller number of possibilities than within the previously seen growth pattern, which requires only approximately 108° angles between three atoms. Such a method has already been used by Boustani *et al.*,[12] who started from Li_8 (T_d) (no PBP) to obtain $Li_{10}(C_{2v})$ (2 PBP)

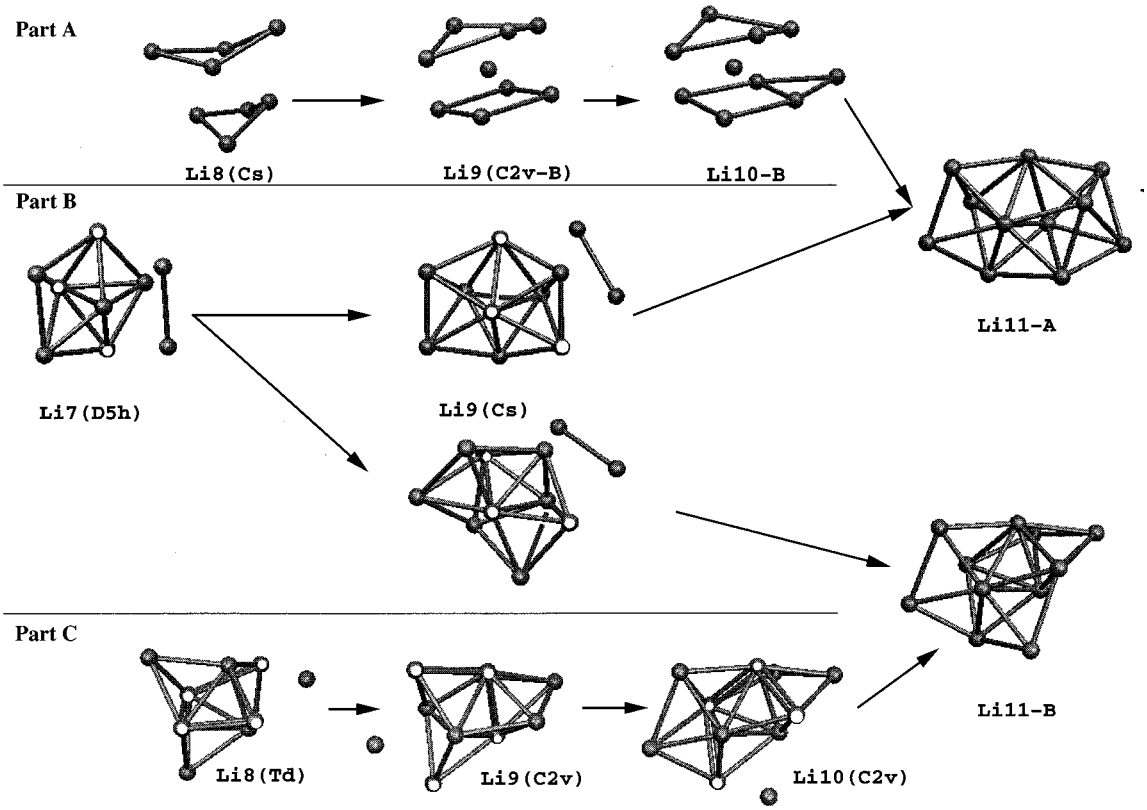

FIG. 2. Pentagonal growth patterns of Li_n clusters from Li_7 to Li_{11}. All the proposed structures have been optimized at the LSD level.

by closing two ''4 atom incomplete pentagons'' (''4AIP''). Nevertheless, as underlined in Ref. 12, this method, when applied up to Li_{14}, leads to a saddle point $Li_{14}(C_{3v})$ by closing 6 ''4AIP.'' In our work, this growth pattern starting from $Li_8(T_d)$ leads to: $Li_9(C_{2v})$, $Li_{10}(C_{2v})$, $Li_{11}B$ (1, 2, and 3 ''4AIP'' are closed successively). The closure of four ''4AIP'' probably yields an unstable structure, since the calculation does not converge after more than 250 geometry steps in the geometry optimization process. Finally, the stable structure of Li_{12} proposed by Sugino *et al.*[17] is found ($Li_{12}S$), starting from $Li_{11}A$ whereas a new stable structure for Li_{13} [$Li_{13}(C_1)$] is obtained starting from $Li_{12}S$ (Fig. 3).

4. Growth without increase of the number of pentagons

Finally, in order to confirm the relevance of the pentagonal growth model, a few Li_n geometries were optimized, starting from the Li_{n-1} optimal structure, by arbitrarily adding one Li atom (i.e., with no increase of the number of PBP). Starting from $Li_8(C_s)$ without any pentagons (part A of Fig. 2), a new $Li_9(C_{2v})$ isomer is obtained (Li_9C_{2v}-B) and after a geometry optimization difficult to drive, one obtains an Li_{10} isomer exhibiting five Li coplanar atoms. Finally Li_{11}-A appears again, with three pentagons. Although stable Li_n geometries can exist without any pentagonal cycle [another illustration is the Li_{13} isomer of Kawai *et al.*[41] ($Li_{13}Kw$)], the natural trend of such structures seems to be the formation of many pentagonal subunits.

5. Li_{18} to Li_{20}

According to the preceding results, a Li_{18} structure with a maximum number of pentagonal subunits is a good candidate to build a new stable isomer. Starting from the stable double icosahedral structure of Li_{19} proposed by Koutecký *et al.*[42] and called $Li_{19}(D_{5h})$ (Fig. 4), one atom is ''removed,'' leading to a new stable Li_{18} isomer: $Li_{18}(C_{5v})$ structure. Closing one ''4AIP'' of $Li_{19}(D_{5h})$, we obtain a new stable Li_{20} isomer: $Li_{20}(C_{2v})$ (Fig. 4). Adding two Li atoms following the mechanism detailed in Sec. II C 2 we have obtained another Li_{20}: $Li_{20}(C_s)$ (Fig. 4). The growth patterns proposed in Secs. II C 2 and II C 3 are relevant, at least until Li_{20}.

It is worthwhile to note the presence of an icosahedral subunit in $Li_{18}(C_{5v})$. We will discuss this point in Sec. IV.

6. Vibrational frequencies

For each new isomer built by PBP subunits [($Li_{11}A$, $Li_{11}B$, $Li_{13}(C_1)$, $Li_{13}(C_s)$, $Li_{18}(C_{5v})$, $Li_{20}(C_{2v})$, $Li_{20}(C_s)$] we have checked the nature of the state (minimum energy or saddlepoint). For this purpose, the Li_{20} structures excepted, all vibrational frequencies (and intensities) were calculated for $Li_{18}(C_{5v})$, they have been carried out with the Gaussian code.[48] Results are reported in Tables II, III, and IV which show that all the corresponding structures are stable. The two Li_{20} structures (carried out with ADF code[36]) are true minima because the number of negative values in the Hessian matrix is checked during the optimization process.

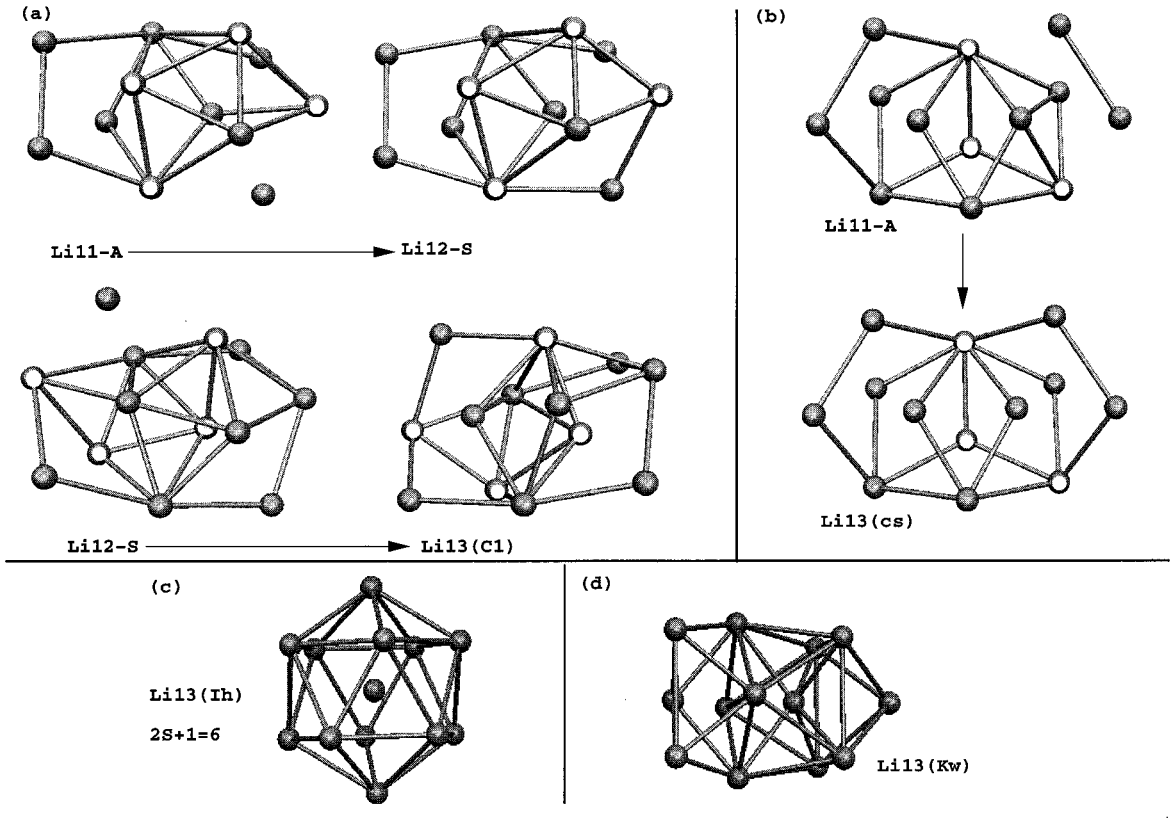

FIG. 3. (a) and (b) Pentagonal growth patterns of Li_n clusters from Li_{11} to Li_{13}. (c) and (d) Two other stable isomers of Li_{13}. All these structures have been optimized at the LSD level.

7. Conclusion

We have obtained new stable PBP structures for $n=11,13,18,20$: [$Li_{11}A$, $Li_{11}B$, $Li_{13}(C_1)$, $Li_{13}(C_s)$, $Li_{18}(C_{5v})$, $Li_{20}(C_{2v})$, $Li_{20}(C_s)$]. Consequently, at least one structure containing a maximum of PBP subunits is known for all size $n=9$ to 14 and $n=18$ to 20. According to the preceding discussion (cf. Sec. II C 1), these structures should probably lie among the most stable ones.

On the other hand, several isomers are known for the sizes $n=9,11,13,18,20$. It is necessary to study the relative stability between them.

D. Relative stability of small lithium cluster isomers

1. Introduction

We focus now on the relative stability among the structures described above, as well as the previous ones given in the literature.

We first examine the relative stability of the very small lithium clusters Li_5, Li_6, Li_8, and Li_9 isomers, which are well known to be critical cases since high-level CI calculations,[12,14,32] have shown quasidegeneracies within less than 0.1 eV. Of course, the LSD approximation is a model too crude to describe unambiguously such a property. Accordingly, these clusters allow us to investigate which combinations of approximate functional are the best for the description of small lithium clusters properties. Then, the conclusions of these tests are used to determine the relative stability of bigger lithium clusters.

2. Relative stability of very small clusters

The differences between the total energies of each isomer obtained with various gradient-corrected functionals at the geometries optimized at the LSD level of approximation are drawn in Fig. 5. Zero point energy (ZPE) contributions are not taken into account here, since their differences lie within a range of a few 0.1 mH,[12] so that they can be neglected. For a better understanding of the diagram, energy differences smaller than 1 mH are rounded off to 0.1.

Figure 5 show that the relative stability is driven by the correlation functional rather than the exchange one. This phenomena can also be observed for bigger clusters (Fig. 6). Consequently, we used in the following only three of the most popular couples of functionals, namely: B88-LYP, B88-P86, and PW91-PW91.

With this reduced set of functionals, optimized geometries of the small clusters have been obtained at the NLSD level. Li_6 (C_{2v}) excepted (as already pointed out; cf. Sec. II B), they are close to the structures calculated at the local level and do not deserve more comments.

The relative stabilities are gathered on Fig. 7. Two combinations of functionals (PW91-PW91, B88-P86) give

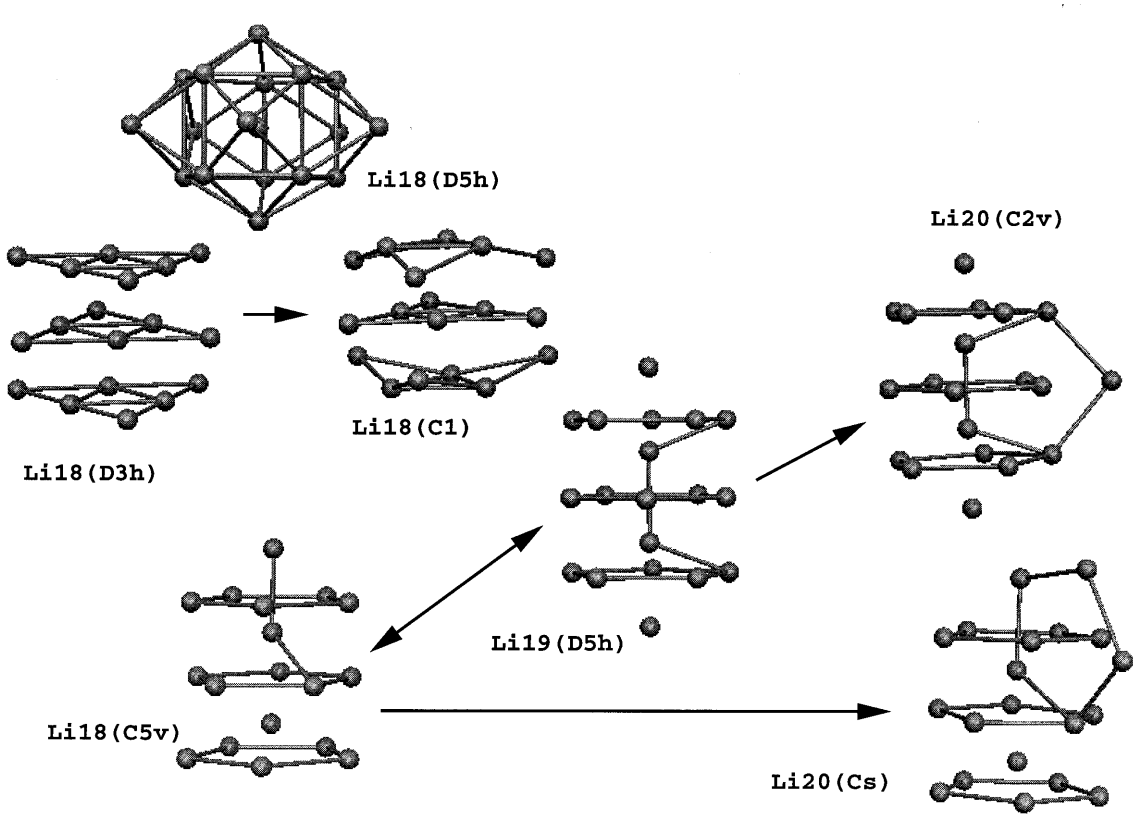

FIG. 4. Three Li_{18} isomers, $Li_{18}(D_{5h})$ (Ref. 42), $Li_{18}(D_{3h})$ (Ref. 42), $Li_{18}(C_{5v})$, and pentagonal growth patterns from Li_{18} to Li_{20}. Note that $Li_{18}(C_{5v})$ has been obtained from $Li_{19}(D_{5h})$ (Ref. 42) and that $Li_{18}(D_{3h})$ leads to $Li_{18}(C_1)$ when the symmetry constraints are removed. All of these structures have been optimized at the LSD level.

Li_5-Bi, $Li_6(C_{2v})$, $Li_7(D_{5h})$, $Li_8(T_d)$, and $Li_9(C_s)$ as the most stable isomers, in agreement with one of the best at the moment *ab initio* calculations.[12,14,32]

In four cases among six, B88-LYP fails. This point is relatively surprising, because this combination of functionals is often considered presently as one of the best.[40] In fact, the quality of the basis sets may be questioned because the LYP correlation functional is known to be more sensitive to the basis set quality.[25] Indeed, the quality of the auxiliary basis set used here (cf. Sec. II A) may be not fully satisfactory for such a functional. Nevertheless, to avoid uncertainty in the following, it has not been retained for the study of the relative stability of larger clusters.

Finally, this study for very small clusters leads to a first conclusion: with the basis set used, only PW91 and P86 correlation functionals are fully satisfactory, whatever the exchange functional selected.

A second conclusion can be deduced from the comparison of Figs. 5 and 7, which gives the difference for a given NLSD functional between the total energies calculated at the LSD and NLSD optimized geometries. This difference represents the error introduced when geometries are only optimized at the LSD level of approximation. A statistic of this error is reported in Fig. 8. One can see that in most cases, the error is less or equal than 2 mH. Only one calculation yields a large energy difference: 12 mH for Li_5 with B88-P86. Consequently, for a given NLSD functional, we can consider that the NLSD total energy differences between two isomers, calculated at the LSD geometry and greater than 2 mH, indicate with confidence the order of stability one would get within a geometry optimization at the NLSD level.

3. Relative stability of Li_n clusters ($9 \leqslant n \leqslant 13$)

According to the preceding conclusions, we have used B88-P86 and PW91-PW91 gradient-corrected functionals to study the relative stability of Li_n clusters ($9 \leqslant n \leqslant 13$). Results are gathered on Fig. 9. For a given NLSD functional, an energy difference lying inside the ± 2 mH ''band'' does not give any information (the only way in this case is to perform geometry optimization at the NLSD level for both considered isomers).

Consequently, only the PW91-PW91 gradient-corrected functional permits to conclude in all cases and one can see that (Fig. 9): (i) $Li_9(C_{2v}-B)$ is less stable than $Li_9(C_{2v})$ and $Li_9(C_s)$. This latter is more stable than $Li_9(C_{2v})$ (Fig. 7). (ii) $Li_{10}(C_{2v})$ is more stable than Li_{10}-B. (iii) Li_{11}-A is more stable than Li_{11}-B. (iv) $Li_{13}(I_h)$ is the most stable among all Li_{13} structures. Moreover, the icosahedron Li_{13} with a multiplicity equal to 6 is found more stable than the cuboctahedron one (2 or 6 multiplicity), in agreement with the result of Pacchioni *et al.*[43]

4. Relative stability for Li_{18} and Li_{20}

The case of Li_{18} isomers has already been investigated by Koutecký *et al.*[42] who found two stable conformations:

TABLE II. Vibrational frequency (in cm^{-1}) and corresponding intensity (in km mol^{-1}) for Li_{11}-*A* and Li_{11}-*B* calculated with LSD (Dirac-VWN) functional [deMon code (Ref. 35)].

	Li_{11}-*A*		Li_{11}-*B*	
No.	Vibrational frequency (cm^{-1})	Approximate intensity (km mol^{-1})	Vibrational frequency (cm^{-1})	Approximate intensity (km mol^{-1})
1	40	0.6	30	0.5
2	80	0.5	70	0.3
3	90	0.5	70	0.6
4	110	0.7	90	2
5	130	1	110	0.7
6	150	2	130	0.3
7	160	2	150	2
8	160	1	160	2
9	170	0.6	170	0.3
10	180	8	180	0.2
11	190	5	180	1
12	190	1	190	3
13	190	2	190	1
14	200	2	200	1
15	210	6	200	4
16	210	4	210	0.3
17	210	4	220	4
18	230	3	230	6
19	240	2	240	1
20	250	1	250	1
21	250	2	260	2
22	260	0.2	270	4
23	260	2	290	0.8
24	280	4	290	6
25	290	3	300	2
26	290	2	320	6
27	310	4	340	1

TABLE III. Vibrational frequency (in cm^{-1}) and corresponding intensity (in km mol^{-1}) for Li_{13}-(C_s) and Li_{13}-(C_1) calculated with LSD (Dirac-VWN) functional [deMon code (Ref. 35)].

	Li_{13}-(C_s)		Li_{13}-(C_1)	
No.	Vibrational frequency (cm^{-1})	Approximate intensity (km mol^{-1})	Vibrational frequency (cm^{-1})	Approximate intensity (km mol^{-1})
1	30	0.2	40	0.6
2	50	1	60	0.1
3	70	0.1	80	2
4	80	0.7	90	0.4
5	90	0.4	100	0.7
6	100	1	120	1
7	110	2	140	1
8	130	0.4	150	2
9	140	3	160	1
10	150	2	160	0.4
11	160	1	170	1
12	170	5	170	0.4
13	175	1	180	2
14	190	3	185	2
15	190	0.3	190	2
16	200	7	200	1
17	200	1	200	1
18	200	0.3	210	2
19	210	2	210	1
20	210	5	210	4
21	220	1	220	1
22	230	1	230	5
23	230	10	240	4
24	240	4	250	17
25	240	3	260	20
26	250	4	260	8
27	250	10	280	5
28	280	5	280	12
29	285	1	290	0.1
30	300	0	300	5
31	320	0.1	320	4
32	370	0.8	330	0.2
33	520	0.2	330	5

$Li_{18}(D_{5h})$ and $Li_{18}(D_{3h})$. We propose $Li_{18}(C_{5v})$ (Fig. 4) which is found, using PW91-PW91, more stable than the D_{5h} and D_{3h} conformations (Table V). Moreover, we find that $Li_{18}(D_{3h})$ undergoes a distortion, leading to $Li_{18}(C_1)$, when the symmetry constraint is removed.

The two Li_{20} isomers proposed in this work (cf. Sec. II C 5) lie very close in energy (Fig. 4), the C_{2v} structure being more stable than the C_s one (LSD binding energy $=1.06$ hartree and 1.04, respectively).

5. Conclusion

For sizes from 5 to 14 and 18 to 20, the most stable isomers among the known structures (from this work or literature) are summarized in Table VI. It is now possible to compute ionization potentials and binding energies of small lithium clusters and compare them with available experimental data and other theoretical approaches (cf. Sec. III).

E. Multiplicity of the cluster

In all cases the most stable geometry is found to exhibit the lowest spin multiplicity (singlets or doublets, cf. Table VI) with the special exception of the Li_{13} cluster. For this last one, different geometries have been found as (local) minima for the doublet multiplicity: (i) $Li_{13}(C_1)$ (cf. Sec. II C 3); (ii) $Li_{13}(C_s)$ (cf. Sec. II C 2); (iii) $Li_{13}(Kw)$, (cf. Sec. II C 2 and Ref. 41). But the icosahedral geometry exhibits the lowest energy with the $2S+1=6$ multiplicity (cf. Sec. II D 3). This multiplicity is in agreement with Hund's rule for the I_h symmetry since the HOMO, which holds five electrons, belongs to the h_u irreducible representation. A lower multiplicity would have lead to a Jahn–Teller distortion lowering the I_h symmetry. One has to recall that the geometry optimization was performed without any symmetry constraint. It is interesting to underline that this result is in contradiction with the results found for Na_{13} cluster,[16,21] for which the $Na_{13}(C_1)$ structure [very similar to $Li_{13}(C_1)$ and named $Na_{13}(a)(C_1)$ in Ref. 16] is more stable than the (hexuplet) icosahedron. This would indicate that the Li_{13} cluster should exhibit paramagnetic properties which are absent from other similar alkali-metal clusters. However, the energy difference between the icosahedron and $Li_{13}(C_1)$ or $Li_{13}(Kw)$ is rather small [ca. 0.1 eV with PW91-PW91 or P88-P86 functional (Fig. 9)] so that we intend to perform further calculations in order to validate

TABLE IV. Vibrational frequency (in cm^{-1}) and corresponding intensity (in km mol^{-1}) for $Li_{18}(C_{5v})$ calculated with LSD (Dirac-VWN) functional [GAUSSIAN 92 code (Ref. 50)].

	$Li_{18}(C_{5v})$	
No.	Vibrational frequency (cm^{-1})	Approximate intensity (km mol^{-1})
1	70	0.0
2	70	0.0
3	100	0.0
4	100	0.0
5	120	0.0
6	140	0.1
7	140	0.1
8	150	0.2
9	155	0.1
10	150	0.0
11	160	0.0
12	160	0.0
13	170	0.0
14	180	0.6
15	180	1
16	190	0.1
17	190	2
18	190	0.0
19	190	2
20	200	1
21	210	3
22	210	1
23	210	0.0
24	215	0.2
25	220	34
26	225	29
27	230	2
28	230	4
29	240	0.0
30	240	0.2
31	240	0.3
32	250	0.0
33	250	0.0
34	270	4
35	270	2
36	290	0.2
37	300	1
38	300	21
39	310	0.0
40	320	0.1
41	320	1
42	330	0.0
43	330	6
44	340	9
45	340	10
46	370	0.4
47	370	0.5
48	395	0.0

this result. Such a validation is possible from an experimental point of view: according to the very small energy differences between the isomers, since the icosahedron is predicted to be a stable structure, it may be detected in a molecular beam through a Stern–Gerlach-type experiment, because of its high magnetic moment, even if it is not the most stable isomer.

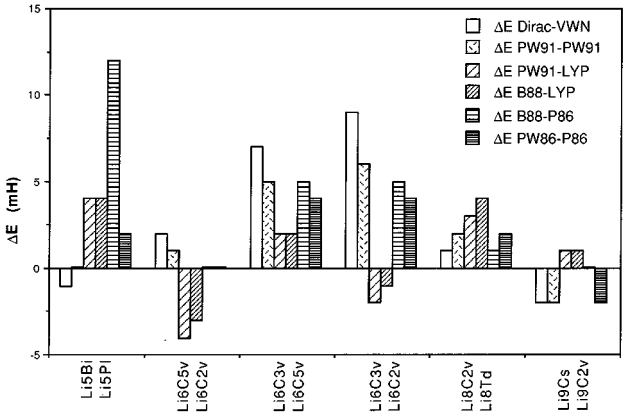

FIG. 5. Total energy differences ΔE (in mH) between two Li_n isomers from Li_5 to Li_9. The total energies of the clusters have been calculated with several gradient-corrected functionals at the LSD geometries.

III. ELECTRONIC PROPERTIES

A. Bond energies

In Figs. 10(a) and 10(b) are reported the bond energies of the Li_n clusters, defined as $E_b = E_1 - (E_n/n)$, where E_1 is the total energy of a single atom, and E_n is the total energy of the n-atoms cluster. When several structures have been found for a given n (isomers) they are all reported in the Fig. 10, the line connecting the (most stable) structures being drawn just for guiding the eyes. The whole set of data is summarized in Table VII. As expected, the bond energy increases with the cluster size, and exhibits an odd–even alternation pointed out by experimentalists.

Since it is well known (cf. Sec. I) that the LSD approximation overestimates the bond energies, we are not surprised to see in Fig. 10(a) that the values calculated with the Dirac-VWN couple of (local) functionals are the largest ones. More interesting is the quite regular trend, including the odd–even modulation, given by most couples of exchange-correlation functionals. However the results are typically smaller by ca. 0.05 eV (PW86-P86), 0.1 eV (PW91-LYP) to 0.25 eV (B88-LYP) off the experiment, whereas the LSD ones are slightly

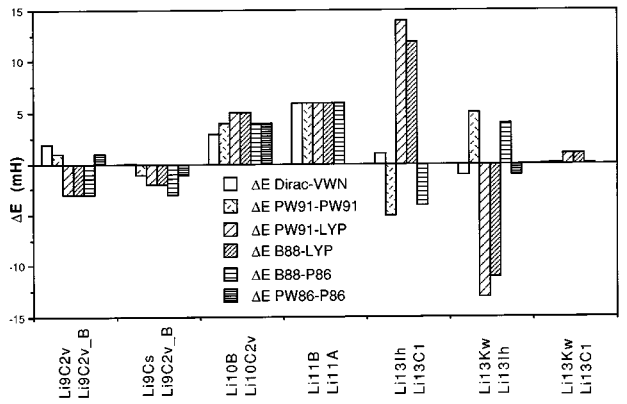

FIG. 6. Total energy differences ΔE (in mH) between two Li_n isomers from Li_9 to Li_{13}. The total energies of the clusters have been calculated with several gradient-corrected functionals at the LSD geometries.

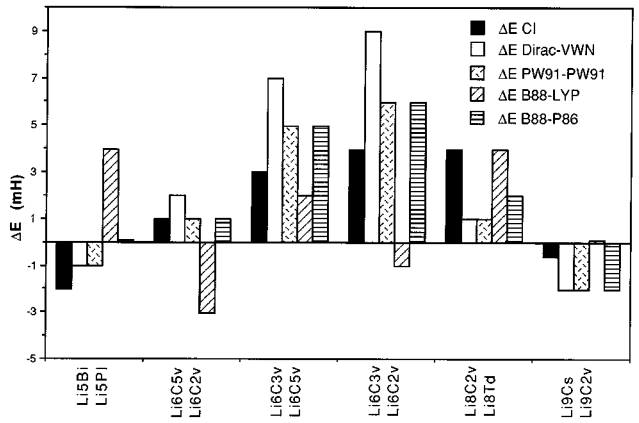

FIG. 7. Total energy differences ΔE (in mH) between two Li_n isomers from Li_5 to Li_9. For each functional, the total energy is calculated at the geometry optimized self-consistently.

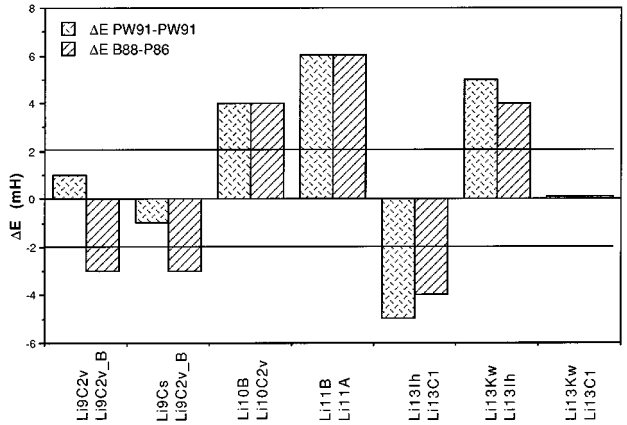

FIG. 9. Total energy differences ΔE (in mH) between two Li_n isomers from Li_9 to Li_{13} calculated with the two functionals: PW91-PW91 and B88-P86 (see text).

overestimated for the biggest clusters, but a bit underestimated for the lightest clusters ($n \leqslant 6$). In all cases the inclusion of gradient corrections leads to a decrease of the bond energies, as expected, but significantly smaller than for usual bond energies since the decrease found in this study lies within the 10%–30% range. All the energies reported in Fig. 10 are calculated at the geometries optimized at the LSD level of approximation since for all the cases we examined within a self-consistent geometry optimization (i.e., with a gradient-corrected potential), the difference in the total energies caused by the change in the geometry remains smaller than 0.06 eV (cf. Sec. II C), underlining in the same time the flatness of the potential energy surface.

A closer look over the data gathered in Fig. 10 and Table VII, reporting CI,[28] MP2[45] and experimental results[8] lets extract some trends among the gradient-corrected functionals:

(i) The bond energy is mainly driven by the exchange functional: this is not unexpected since the exchange energy is almost one order of magnitude larger than the correlation energy. One can also notice that the gradient-corrected functionals for exchange proposed by Perdew–Wang PW86[26] and PW91[28] lead to close energies (in agreement with the fact that both are parametrized on the electron gas), whereas the Becke 88[27] functional leads to smaller energies, whatever the correlation functional is.

(ii) The correlation functional is more important for some modulation between the different sizes. In particular, the shell structure of the clusters, i.e., the larger stability of $n=2,8,\ldots$ clusters, is mainly recovered by the correlation functional. For this purpose the LYP functional looks better than P86 or PW91 correlation functionals. This is mostly apparent in the Li_2 dimer.

Since the CI accuracy cannot be obtained for bigger clusters within this formalism, the interest of our calculations increases with the size of the clusters. This is related to the necessity to limit the CI expansion because of computing limitations, whereas Koutecký underlined the necessity to use high quality MR-CI for a correct description of the Li_n clusters. Because of the computational cost of such an approach (n^7) compared to the DFT (n^3), the CI approach has to be dropped for bigger clusters.

From a pragmatic point of view one can conclude that, among the couples of functionals tested in this work, the PW91-LYP leads to bond energies closer to experiment than

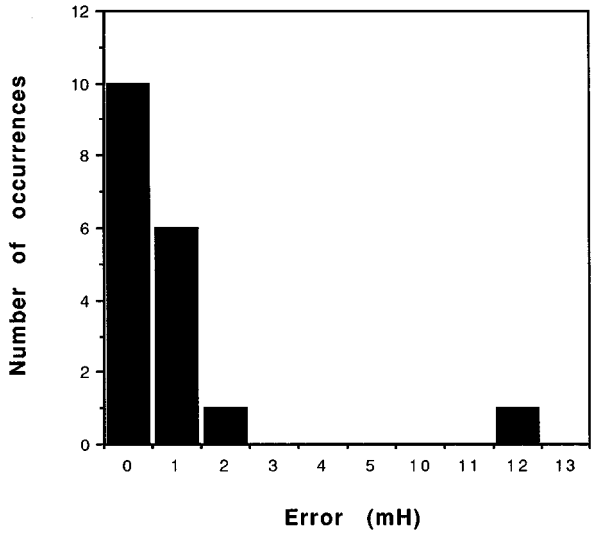

FIG. 8. Histogram of errors (in mH) of the total energy differences between two isomers, for three sets of gradient-corrected functionals (PW91-PW91, B88-LYP, and B88-P86). These errors stem from the change in geometry caused by the optimization: optimization within the LSD approximation, or with the given gradient-corrected functional.

TABLE V. PW91-PW91 total energy (in hartrees) for the three Li_{18} isomers.

Cluster	Total energy
$Li_{18}(C_{5v})$	−135.210
$Li_{18}(D_{5h})$	−135.189
$Li_{18}(C_1)$	−135.204

TABLE VI. Lithium clusters structures (Li_n), as determined in this work and previously in the literature, for $n=2-14$, 18–20. The star indicates the most stable isomer. The stability is confirmed by vibrational analysis or check of the Hessian matrix.

Structure	Visible Fig.	Stability: Confirmed (Ref.)	Stability: Saddle point	Stability: Not determined	Spin multiplicity
$Li_2(D_{\infty h})$	1	(*) This work			1
$Li_3(C_{2v})$	1	(*) 12			2
$Li_4(D_{2h})$	1	(*) 12			1
Li_5-Pl	1	12			2
Li_5-Bi	1	(*) 12			2
$Li_6(C_{5v})$	1	12			1
$Li_6(C_{2v})$	1	(*) 12			1
$Li_6(C_{3v})(\approx D_{3h})$	1	12			1
$Li_7(D_{5h})$	1	(*) 12 and this work			2
$Li_8(T_d)$	1	(*) 12			1
$Li_8(C_{2v})(\approx D_{2d})$	1	12			1
Li_8 (C_s)	2			×	1
$Li_9(C_{2v})$	2	12			2
$Li_9(C_s)$	2	(*) This work			2
$Li_9(C_{2v}-B)$	2	This work			2
$Li_{10}(C_{2v})$	2	(*) 12 and this work			1
(Li_{10}-B)	2			×	1
Li_{11}-A	2	(*) This work			2
Li_{11}-B	2	This work			2
Li_{12}-S	3	(*) 17			1
$Li_{13}(C_1)$	3	This work			2
$Li_{13}(C_s)$	3	This work			2
$Li_{13}(K_w)$	3	41			2
$Li_{13}(O_h)$	3	This work			6
$Li_{13}(I_h)$	3	(*) 43			6
$Li_{14}(C_{3v})$			×		1
$Li_{18}(D_{5h})$	4	42			1
$Li_{18}(D_{3h})$	4	42			1
$Li_{18}(C_1)$	4			×	1
$Li_{18}(C_{5v})$	4	(*) This work			1
$Li_{19}(D_{5h})$	4	41			2
$Li_{20}(C_{2v})$	4	This work			1
$Li_{20}(C_s)$	4	This work			1

other sets of functionals, whereas the B88-LYP, considered as one of the best ones by some authors,[40] leads to bond energies significantly worse. One can also remark that the strong diminution of the increase of the bond energy when passing from Li_4 to Li_5 is in agreement with the CI calculation, but not with experiment.

B. Ionization Potentials (IP)

In Fig. 11 are reported vertical IP of Li_n clusters calculated within various functionals in regard to experimental data and, when available, CI calculations. They are obtained as differences of n electron and $n-1$ electron total energy calculations. When different isomers are known, all data—which are gathered in Table VIII—are reported. The line between the points connects the most stable isomers. In order to picture the following comments, Fig. 11 has been arbitrarily split into two parts to reduce the overlap of the curves. From these data some comments related to the odd–even alternation, the geometry of the cluster and the nature of the selected functional for the description of the IP can be extracted.

(i) The odd–even alternation of the IP, which is well known in the cluster physics, in particular for alkali metals, is clearly reproduced by all the functionals, including the LSDA (Dirac-VWN exchange-correlation functional[38]), although it is smoother for big clusters than experiment. The smoothing starts for clusters Li_n with $n>10$, and may be related to the existence of an increasing number of isomers (*vide infra*) with n. In other words the calculations may have not necessarily converged to the most stable structures for $10 \leqslant n \leqslant 13$.

(ii) It appears that the LSDA (Dirac–VWN) overestimates all the IP by an amount starting from 0.3 eV for Li_2 and reaching a value of ca. 0.7 eV for Li_{10} and larger clusters. This was not really expected since the LSDA describes quite well the IP of Na clusters, as pointed out by Martins *et al.*[44] This underlines the necessity to handle a more accu-

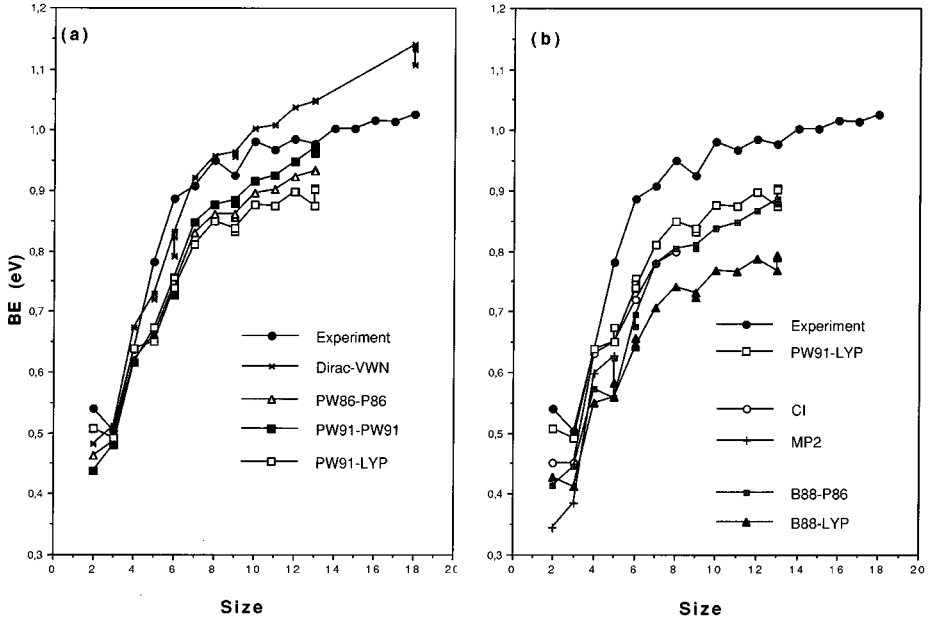

FIG. 10. Atomization energies (in eV/atom) of small Li_n clusters calculated with LSD (Dirac–VWN) and various NLSD functionals. For sake of comparison the CI (Ref. 14) (when available) and MP2 (Ref. 49) values as well as experimental values (Ref. 7), are also reported.

rate exchange-correlation functional for Li clusters for which the correlation (in the *ab initio* sense) plays a more important role[13] than for Na clusters.

(iii) Similar results are obtained with all the gradient approximations used in this work for small clusters, namely $n \leqslant 10$. One can see easily from Table VIII that for bigger clusters, the PW91-LYP and B88-LYP couples lead to better agreement with the experimental trends than other couples of functionals. According to the results relative to the properties discussed above, the PW91-LYP exchange-correlation functional looks to be the best choice for the description of the lithium clusters. This is rather unexpected since the PW91

TABLE VII. Atomization energy (in eV) calculated with LSD (Dirac–VWN) and various NLSD functionals. For sake of comparison the CI (Ref. 14), MP2 (Ref. 49), and experimental values (Ref. 7) are reported.

Cluster	E_b (Dirac–VWN)	E_b (PW86-P86)	E_b (PW91-PW91)	E_b (B88-P86)	E_b (B88-LYP)	E_b (Pw91-LYP)	E_b (Exp.)	E_b CI	E_b MP2
Li	0.00	0.00	0.00	0.00	0.00	0.00	0.00	0.00	0.00
Li_2	0.48	0.46	0.44	0.41	0.43	0.51	0.54	0.45	0.34
$Li_3(C_{2v})$	0.51	0.49	0.48	0.45	0.41	0.49	0.50	0.45	0.39
$Li_4(D_{2h})$	0.67	0.62	0.62	0.57	0.55	0.64	0.64	0.63	0.60
Li_5Bi	0.73	0.66	0.67	0.56	0.56	0.65	0.78	0.65	0.63
Li_5IP	0.72	0.67	0.67	0.62	0.58	0.67			
$Li_6(C_{2v})$	0.83	0.75	0.76	0.70	0.64	0.74	0.89	0.72	
$Li_6(C_{5v})$	0.82	0.75	0.75	0.69	0.66	0.76			
$Li_6(C_{3v})$	0.79	0.73	0.73	0.68	0.65	0.75			
$Li_7(D_{5h})$	0.92	0.83	0.85	0.78	0.71	0.81	0.91	0.78	
$Li_8(T_d)$	0.96	0.86	0.88	0.81	0.74	0.85	0.95	0.80	
$Li_9(C_s)$	0.96	0.86	0.88	0.81	0.73	0.84	0.93		
$Li_9(C_{2v}-B)$	0.96	0.86	0.88	0.81	0.72	0.83			
$Li_{10}(C_{2v})$	1.00	0.90	0.92	0.84	0.77	0.88	0.98		
Li_{11}-A	1.01	0.90	0.93	0.85	0.77	0.88	0.97		
Li_{12}-S	1.04	0.92	0.95	0.85	0.79	0.90	0.98		
$Li_{13}(I_h)$	1.05	0.93	0.97	0.89	0.77	0.88	0.98		
$Li_{13}(C1)$	1.05	0.93	0.96	0.88	0.79	0.90			
$Li_{13}(Kw)$	1.05	0.93	0.96	0.88	0.79	0.90			
Li_{14}							0.98		
Li_{15}							1.00		
Li_{16}							1.00		
Li_{17}							1.02		
$Li_{18}DbIco$	1.14						1.02		
$Li_{18}D_{3h}$	1.13								
$Li_{18}D_{5h}$	1.11								

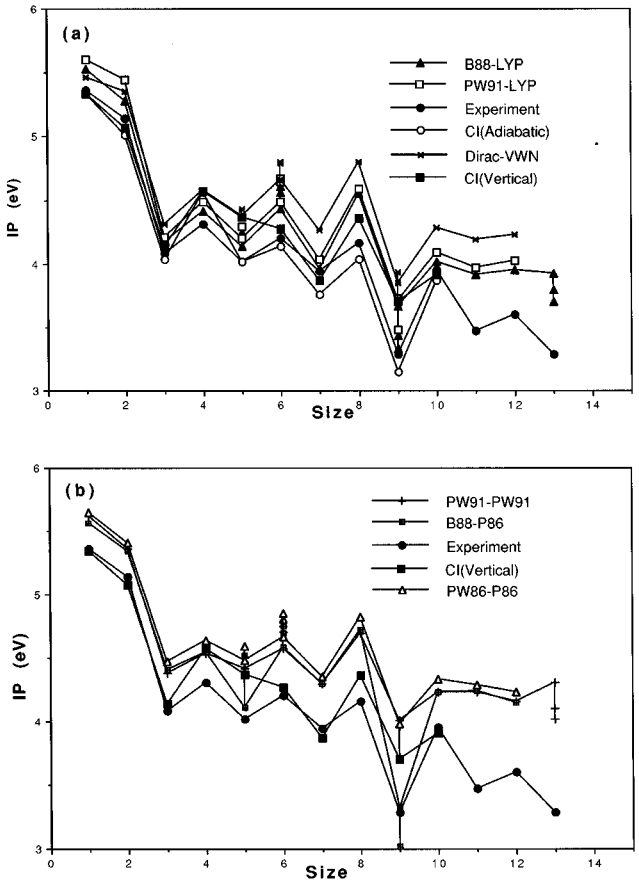

FIG. 11. Vertical ionization potential (in eV) calculated with LSD (Dirac–VWN) and various NLSD functionals. For sake of comparison the vertical and adiabatic CI ionization potentials (when available) (Ref. 14) and experimental values (Ref. 9) are reported.

correlation functional has been designed partly for compensating the PW91 exchange functional deficiencies. The LYP functional, although it does not admit the homogeneous gas limit for small gradients, was expected to be a good correlation functional for the description of clusters of very light elements such as lithium, typically an inhomogeneous electronic system.

However, there is not much satisfaction when it is coupled to the B88 functional, although this is often done in present calculations in the literature. This could be related to the large enhancement factor of the B88 functional for large values of the reduced density gradient (relatively to the local exchange), a factor which is (on the contrary) damped by the PW91 exchange functional.

(iv) Comparison to the jellium-LDA model: In Fig. 12 are reported the IP calculated within the spherical jellium model.[8] Most of the discrepancy, which amounts to 38% for Li_{18}, is mainly due to the jellium approximation since the LDA gives only 12% of discrepancy in our Li_{18} calculation [the difference between the LDA functional retained in Ref. 8, namely Dirac–Wigner,[37,45] with the one used in our calculation (Dirac–VWN), should be negligible]. Let us recall that with the gradient corrected functional, the discrepancy is reduced to 8% for the same cluster.

It is interesting to put in regard the eigenvalues of the jellium-LDA[46] calculation with the corresponding valence ones extracted from our calculation in Figs. 13(a) and 13(b). For this purpose we selected the eigenvalues of our LSD and NLSD (B88-LYP) calculations, and reported them in correspondence to the spherical jellium model, in which the orbitals are labelled according to the S,P,D labels. The identification is quite easy because of the large gap between the s orbital from the average of the three p ones and the average of the five d ones. To be correct, one should count the nodal surfaces of the MOs for labeling the orbitals, but the knowledge of the energetic positions is sufficient to assign the orbitals.

Since the orbitals should belong to a subgroup of R^3, this identification should not hold for clusters exhibiting D_{5h} or I_h symmetry (Li_7 or Li_{13}). This explains the apparent discontinuity of the curves reported in Fig. 13(a). For sake of comparison, the eigenvalues of the jellium-LDA calculations for Na_n clusters[47] and the corresponding NLSD (with molecular dynamics[21]) values are also reported in Fig. 13(b).

Starting from Figs. 12 and 13 of the present work and Fig. 29 of Ref. 4, it is clear that the jellium-LDA leads to a crude description of electronic structures of small Li_n clusters, although it is not the case for Na_n clusters. This failure of jellium-LDA is not due to the LDA approximation (*vide supra*) but could be related to the too small value of Wigner–Seitz radius for lithium ($r_s=3.28$ a.u.), contrarily to the case of the sodium ($r_s=4$ a.u.).[11] More precisely, r_s represents the equilibrium valence electron density for a given material and it can be demonstrated that the jellium model ''works'' well only near $r_s=4$ a.u.[11] One reason of this difference between Li and Na could originate in the difference between the core-valence electronic interactions for these two metals. For example, a great difference exists between the effective electron mass of Li and Na for both bulk and small clusters.[3] Perhaps, the use of the stabilized jellium model,[48] which is more realistic than the classical jellium model, would lead to a better understanding of this failure. Finally, some differences also have to be expected since the jellium simulates a high temperature cluster, whereas the molecular model describes a rigid structure at 0 K. To be more correct, one should compare the jellium eigenvalues to a thermodynamical average of the molecular eigenvalues, but one should reasonably expect that such approach would not shift sufficiently the spectrum.

IV. CONCLUSION

The results exposed here bring new informations for both the predictive power of DFT and the structural and energetic properties of small Li_n clusters ($n \leqslant 20$).

Our DFT calculations confirm that pentagonal bipyramids (PBP) very often appear in small lithium clusters and two different mechanisms of the pentagonal growth have been proposed. Furthermore, for sizes $n \geqslant 9$, we note that the most stable Li_n isomer contains the greatest number of PBP subunits (Table VI).

This work also brings information about the question of

TABLE VIII. Vertical ionization potential (in eV) calculated with LSD (Dirac–VWN) and various NLSD functionals. For sake of comparison the CI vertical and adiabatic ionization potential (when available) (Ref. 14), experimental values (Ref. 9), and jellium-LDA (Ref. 8) are reported. The relative standard errors are given in percents.

Cluster	IP (Dirac–VWN)	IP (PW86-P86)	IP (PW91-PW91)	IP (B88-P86)	IP (B88-LYP)	IP (PW91-LYP)	IP (Exp.)	Adiabatic IP (CI)	Vertical IP (CI)	IP (jellium-LDA)
Li	5.47	5.65	5.62	5.56	5.53	5.60	5.36	5.34	5.34	
Li_2	5.36	5.41	5.36	5.34	5.28	5.45	5.14	5.01	5.07	6.65
$Li_3(C_{2v})$	4.31	4.47	4.38	4.40	4.18	4.21	4.08	4.03	4.10	4.22
$Li_4(D_{2h})$	4.58	4.64	4.54	4.55	4.41	4.49	4.31	4.56	4.57	4.85
Li_5Bi	4.38	4.48	4.42	4.11	4.14	4.20	4.02	4.02	4.37	5.18
Li_5IP	4.43	4.59	4.50	4.52	4.25	4.29				
$Li_6(C_{2v})$	4.66	4.67	4.57	4.58	4.43	4.49	4.20	4.14	4.27	5.42
$Li(C_{5v})$	4.79	4.80	4.70	4.69	4.56	4.64				
$Li_6(C_{3v})$	4.80	4.85	4.75	4.75	4.60	4.68				
$Li_7(D_{5h})$	4.26	4.35	4.30	4.29	3.96	4.03	3.94	3.76	3.87	5.60
$Li_8(T_d)$	4.80	4.83	4.69	4.72	4.55	4.59	4.16	4.03	4.36	5.72
$Li_9(C_s)$	3.85	3.98	4.01	3.32	3.66	3.71	3.29	3.15	3.70	3.80
$Li_9(C_{2v}-B)$	3.69		3.72	3.02	3.44	3.48				
$Li_{10}(C_{2v})$	4.28	4.33	4.23	4.23	4.02	4.09	3.95	3.87	3.91	4.10
Li_{11}-A	4.19	4.29	4.23	4.24	3.92	3.97	3.47			4.31
Li_{12}-S	4.23	4.24	4.16	4.15	3.95	4.02	3.60			4.49
$Li_{13}(I_h)$			4.31		3.92		3.29			4.64
$Li_{13}(C1)$			4.10		3.79					
$Li_{13}(Kw)$			4.02		3.70					
Li_{14}							3.54			4.76
Li_{15}							3.30			4.85
Li_{16}							3.44			4.94
Li_{17}							3.22			5.03
$Li_{18}DbIco$	4.06						3.31			5.09
$Li_{18}(D_{3h})$										
$Li_{18}(D_{5h})$										
rms deviation	13.1	14.7	13.2	11.8	9.0	10.1		2.4	4.3	29.2

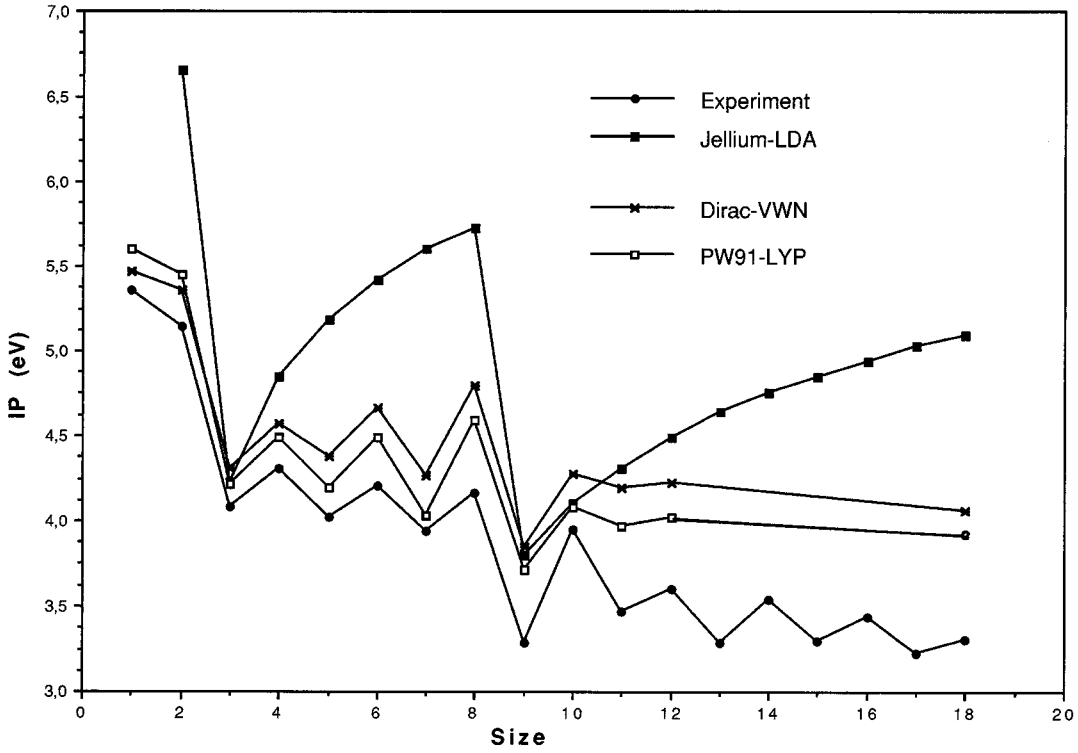

FIG. 12. Vertical ionization potential (in eV) calculated with LSD (Dirac–VWN) and PW91-LYP functional. The jellium-LDA (Ref. 8) and experimental (Ref. 9) results are also reported.

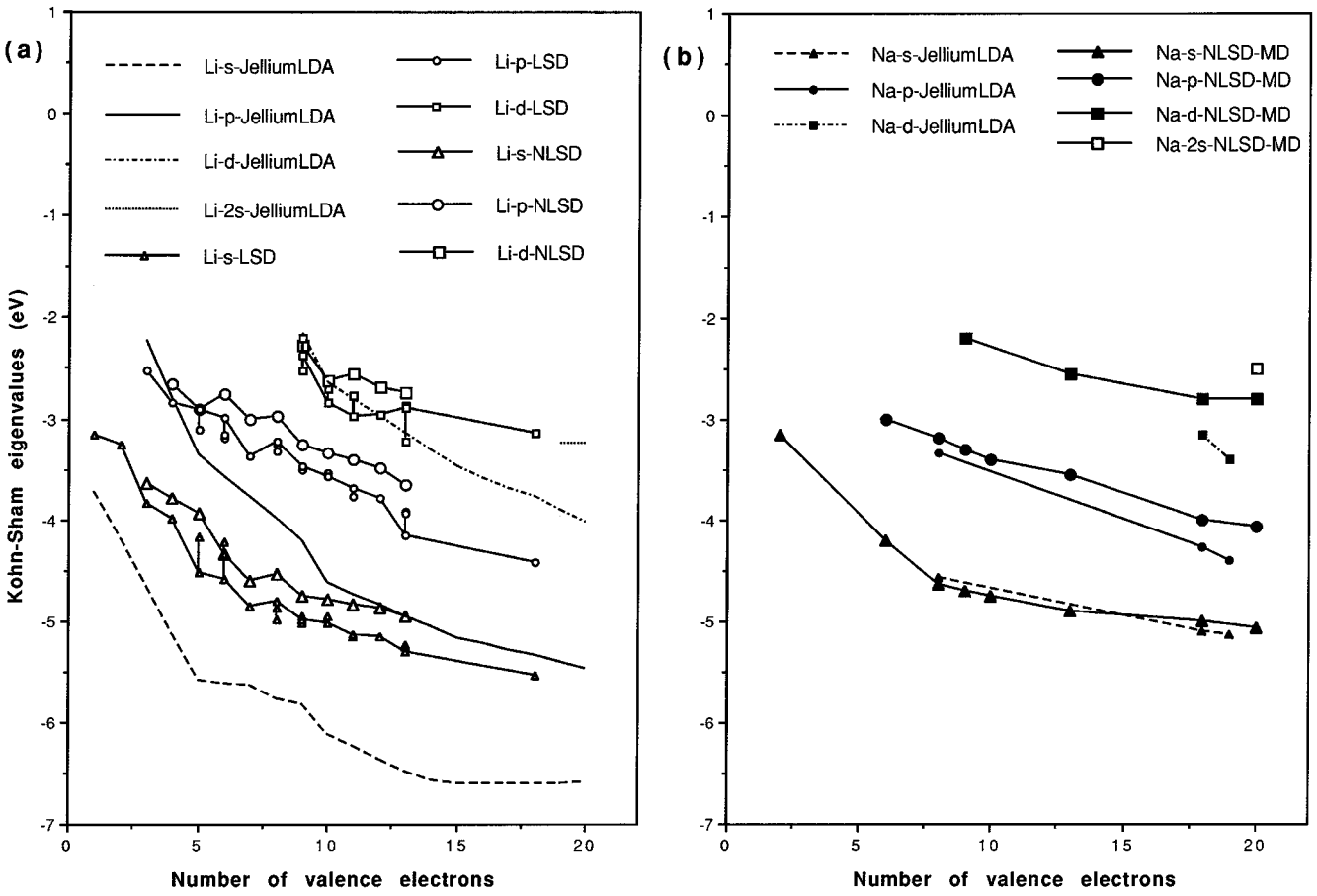

FIG. 13. (a) Kohn–Sham eigenvalues (in eV) for valence orbitals of small Li_n clusters: jellium-LDA for Li, Ref. 46; LSD (Dirac–VWN) and NLSD (B88-LYP) values: this work. (b) Kohn–Sham eigenvalues (in eV) for valence orbitals of small Na_n clusters: jellium-LDA for Na, Ref. 47; NLSD-molecular dynamics values from Ref. 21.

the transition from nonicosahedral to icosahedral packing. This question is important because, similar to the rare gas systems, small Li_n clusters are predicted to form icosahedral structures.[41] But at what size does the icosahedron appear? This point is certainly connected to the great occurrence of PBP in small Li_n clusters. The most recent works[17,41,42] pointed out that this transition takes place between size $n=19$ to $n=26$. According to our results, this transition size may start with the minimum value, i.e., $n=13$, because $Li_{13}(I_h)$ seems to be the most stable Li_{13} isomer at this moment. In fact, as already said, this result must be confirmed by further calculations. Nevertheless, $Li_{18}(C_{5v})$, which contains an icosahedral subunit, is clearly the most stable Li_{18} isomer. Accordingly, the transition may occur for size smaller than 18.

In the second part of this work, ionization potentials and binding energies have been studied in regard to the size and the geometry of the clusters. Our results show the high accuracy of NLSD calculations: in all cases examined, they are as close to experiment as more sophisticated post-Hartree–Fock calculations. Nevertheless, in most cases, the NLSD values are sensitive on the exchange-correlation functional choice. These differences between NLSD functionals can be traced either to the different sensitivity of the functional to the basis set quality or to the different efficiency of the correlation functional itself in correcting the exchange energy deficiency. In fact, it appears that some combinations of gradient-corrected functionals are more successful than others in the description of Li_n clusters: PW91-PW91 or B88-P86 are the best for the relative stability, but PW91-LYP looks better for electronic properties.

It is worthwhile to note that energetic properties do not depend significantly on the geometry of the isomers. This indicates the flatness of the potential energy surface for all the considered sizes. Our DFT all electron calculations clearly improve the jellium-LDA model. They confirm the fact that, contrary to Na_n clusters, this last model leads to a quantitatively inaccurate description of the electronic properties of Li_n clusters. This failure of jellium-LDA in not due to LDA approximation but is related to the jellium model itself.

ACKNOWLEDGMENTS

We are indebted to Professor D. R. Salahub for providing us a copy of the deMon program, Professor M. Broyer and his collaborators, and Professor V. Bonačić-Koutecký, as well as R. Fournier for helpful discussions.

[1] W. D. Knight, K. Clemenger, W. A. de Heer, W. A. Saunders, M. Y. Chou, and M. L. Cohen, Phys. Rev. Lett. **52**, 2141 (1984); **53**, 510(E) (1984).
[2] J. Petersen, S. Bjørnholm, J. Borggreen, K. Hansen, T. P. Martin, and H. D. Rasmussen, Nature **353**, 733 (1991).
[3] M. Broyer and Ph. Dugourd, Comm. At. Mol. Phys. (in press).
[4] W. A. de Heer, Rev. Mod. Phys. **65**, 611 (1993).
[5] *Cluster Models for Surface and Bulk Phenomena*, NATO ASI Series, edited by G. Pacchioni and P. S. Bagus (Plenum, New York, 1992).
[6] C. Brechignac, Ph. Cahuzac, M. de Frutos, J. Ph. Roux, and K. Bowen, *Physics and Chemistry of Finite Systems: From Cluster to Crystals*. NATO ASI Series, edited by P. Jena, S. N. Khanna, and B. K. Rao (Kluwer Academic, Dortrecht, 1992), p. 369.
[7] C. Brechignac, H. Busch, P. Cahuzac, and J. Leygnier, J. Chem. Phys. **101**, 6992 (1994).
[8] B. Vezin-Pintar, Thesis, Université Lyon-I, 1994.
[9] (a) Ph. Dugourd, D. Rayane, P. Labastie, B. Vezin, J. Chevaleyre, and M. Broyer, Chem. Phys. Lett. **197**, 433 (1992); (b) B. Vezin, Ph. Dugourd, D. Rayane, P. Labastie, J. Chevaleyre, and M. Broyer, Chem. Phys. Lett. **206**, 521 (1993).
[10] Z. Penzar and W. Ekart, Z. Phys. D **19**, 109 (1991).
[11] M. Brack, Rev. Mod. Phys. **65**, 677 (1993).
[12] I. Boustani, W. Pewestorf, P. Fantucci, V. Bonačić-Koutecký, and J. Koutecký, Phys. Rev. B **35**, 9437 (1987).
[13] V. Bonačić-Koutecký, P. Fantucci and J. Koutecký, Chem. Rev. **91**, 1035 (1991).
[14] V. Bonačić-Koutecký, J. Gaus, M. F. Guest, L. Češpiva, and J. Koutecký, Chem. Phys. Lett. **206**, 528 (1993).
[15] A. Julg, M. Bénard, M. Bourg, M. Gillet, and E. Gillet, Phys. Rev. B **9**, 3248 (1974).
[16] R. Poteau and F. Spiegelmann, J. Chem. Phys. **98**, 6540 (1993).
[17] O. Sugino and H. Kamimura, Phys. Rev. Lett. **65**, 2696 (1990).
[18] W. Kohn and L. J. Sham, Phys. Rev. A **140**, 1133 (1965).
[19] R. G. Parr and W. Yang, *Density-Functional Theory of Atoms and Molecules* (Oxford University Press, Oxford, 1989).
[20] R. Car and M. Parrinello, Phys. Rev. Lett. **55**, 2471 (1985); proceedings of the NATO ARW: *Simple Molecular Systems at Very High Density*, Les Houches (France), NATO ASI Series (Plenum, New York, 1988), p. 455.
[21] (a) U. Röthlisberger and W. Andreoni, J. Chem. Phys. **94**, 8129 (1991); (b) U. Röthlisberger, W. Andreoni, and P. Giannozzi, *ibid.* **96**, 1248 (1992).
[22] T. Ziegler, Chem. Rev. **91**, 651 (1991).
[23] J. M. Seminario, Chem. Phys. Lett. **206**, 547 (1993).
[24] I. Papai, A. Goursot, A. St Amant, and D. R. Salahub, Theor. Chim. Acta. **84**, 217 (1992).
[25] H. Chermette, A. Lembarki, P. Gulbinat, and J. Weber, Int. J. Quantum Chem. **56**, 753 (1995).
[26] J. P. Perdew and Y. Wang, Phys. Rev. B **33**, 8800 (1986).
[27] A. D. Becke, Phys. Rev. A **38**, 3098 (1988).
[28] J. P. Perdew, in *Electronic Structure of Solids '91*, edited by P. Ziesche and H. Eschrig (Academic Verlag, Berlin, 1991).
[29] J. P. Perdew, Phys. Rev. B **33**, 8822 (1986); **38**, 7406(E) (1986).
[30] C. Lee, W. Yang, and R. G. Parr, Phys. Rev. B **37**, 785 (1988).
[31] Ph. Dugourd, J. Blanc, V. Bonačić-Koutecký, M. Broyer, J. Chevaleyre, J. Koutecký, J. Pittner, J. P. Wolf, and L. Wöste, Phys. Rev. Lett. **67** (19), 2638 (1991).
[32] J. Blanc, V. Bonačić-Koutecký, M. Broyer, J. Chevaleyre, Ph. Dugourd, J. Koutecký, C. Scheuh, J. P. Wolf, and L. Wöste, J. Chem. Phys. **96**, 1793 (1992).
[33] G. Gardet, F. Rogemond, and H. Chermette, Theor. Chim. Acta **91**, 249 (1995).
[34] R. O. Jones, G. Gantefor, S. Hunsicker, and P. Pieperhoff, J. Chem. Phys. **103**, 9549 (1995).
[35] (a) D. R. Salahub, R. Fournier, P. Mlynarski, I. Papai, A. St Amant, and J. Ushio, *Density Functional Methods in Chemistry*, edited by J. K. Labanowski and J. W. Andzelm (Springer, New York, 1991), pp. 77–100; (b) A. St Amant and D. R. Salahub, Chem. Phys. Lett. **169**, 387 (1990); (c) A. St Amant, Ph.D. thesis, Université de Montréal (1991).
[36] (a) E. J. Baerends, D. E. Ellis, and P. Ros, Chem. Phys. **2**, 41 (1973); (b) G. te Velde and E. J. Baerends, J. Comput. Phys. **99**, 84 (1992); ADF release 1.02, Department of Theoretical Chemistry, Vrije Universiteit, Amsterdam.
[37] P. A. Dirac, Proc. Cambridge Philos. Soc. **26**, 376 (1930).
[38] S. H. Vosko, L. Wilk, and M. Nusair, Can. J. Phys. **58**, 1200 (1980).
[39] N. Godbout, D. R. Salahub, J. Andzelm, and E. Wimmer, Can. J. Chem. **70**, 560 (1992).
[40] B. G. Johnson, P. M. W. Gill, and J. A. Pople, J. Chem. Phys. **98**, 5612 (1993).
[41] R. Kawai, M. W. Sung, and J. H. Weare, *Physics and Chemistry of Finite Systems: From Cluster to Crystals*, NATO ASI Series, edited by P. Jena, S. N. Khanna, and B. K. Rao (Kluwer Academic, Dortrecht, 1992), p. 441.
[42] J. Koutecký, V. Bonačić-Koutecký, I. Boustani, P. Fantucci, and W. Pewestorf, *Large Finite Systems*, edited by G. Benedek, T. P. Martin, and G. Pacchioni (Springer Verlag, Berlin, 1987), p. 214.
[43] G. Pacchioni and J. Koutecký, J. Chem. Phys. **81**, 3588 (1984).
[44] J. L. Martins, J. Buttet, and R. Car, Surf. Sci. **156**, 649 (1985).
[45] E. P. Wigner, Phys. Rev. Lett. **46**, 1002 (1934).
[46] M. J. Puska, R. M. Nieminen, and M. Manninen, Phys. Rev. B **31**, 3486 (1985).
[47] W. Ekardt, Phys. Rev. B **29**, 1558 (1984).
[48] J. P. Perdew, H. Q. Tran, and E. D. Smith, Phys. Rev. B **42**, 11 627 (1990).
[49] (a) B. K. Rao and P. Jena, Phys. Rev. B **32**, 2058 (1985); (b) **37**, 2867 (1988); (c) B. K. Rao, S. N. Khanna, and P. Jena, *ibid.* **36**, 953 (1987).
[50] M. J. Frisch, G. W. Trucks, M. Head-Gordon, P. M. W. Gill, M. W. Wong, J. B. Foresman, B. G. Johnson, H. B. Schlegel, M. A. Robb, E. S. Replogle, R. Gomperts, J. L. Andres, K. Raghavachari, J. S. Binkley, J. J. P. Stewart, and J. A. Pople, GAUSSIAN 92/DFT, Gaussian, Inc., Pittsburgh, PA, 1992.